Buckling-Induced Kirigami

Ahmad Rafsanjani[1] and Katia Bertoldi[1,2,*]
[1]John A. Paulson School of Engineering and Applied Sciences, Harvard University, Cambridge, Massachusetts 02138, USA
[2]Kavli Institute, Harvard University, Cambridge, Massachusetts 02138, USA
(Received 3 November 2016; published 21 February 2017)

We investigate the mechanical response of thin sheets perforated with a square array of mutually orthogonal cuts, which leaves a network of squares connected by small ligaments. Our combined analytical, experimental and numerical results indicate that under uniaxial tension the ligaments buckle out of plane, inducing the formation of 3D patterns whose morphology is controlled by the load direction. We also find that by largely stretching the buckled perforated sheets, plastic strains develop in the ligaments. This gives rise to the formation of kirigami sheets comprising periodic distribution of cuts and permanent folds. As such, the proposed buckling-induced pop-up strategy points to a simple route for manufacturing complex morphable structures out of flat perforated sheets.

DOI: 10.1103/PhysRevLett.118.084301

In recent years, origami [1–9] and kirigami [10–27] have become emergent tools to design programmable and reconfigurable mechanical metamaterials. Origami-inspired metamaterials are created by folding thin sheets along predefined creases, whereas kirigami allows the practitioner to exploit cuts in addition to folds to achieve large deformations and create 3D objects from a flat sheet. Therefore, kirigami principles have been exploited to design highly stretchable devices [18–24] and morphable structures [25–27]. Interestingly, several of these studies also show that precreased folds are not necessary to form complex 3D patterns, as mechanical instabilities in flat sheets with an embedded array of cuts can result in out-of-plane deformation [19–26]. However, while a wide range of 3D architectures have been realized by triggering buckling under compressive stresses [25,26], instability-induced kirigami designs subjected to tensile loading are limited to a single incision pattern comprised of parallel cuts in a centered rectangular arrangement [19–23].

In this Letter, we investigate the tensile response of elastic sheets of thickness t perforated with a square array of mutually orthogonal cuts. This perforation pattern introduces a network of square domains of edge l separated by hinges of width δ [Fig. 1(a)]. While the planar response of such perforated sheets in the thick limit (i.e., for large values of t/δ) has received significant attention, as it is characterized by effective negative Poisson's ratio [28–36] [Fig. 1(b)], here we add another dimension and study how the behavior of the system evolves when the thickness is progressively decreased (i.e., for decreasing values of t/δ). Our combined analytical, numerical, and experimental results indicate that in sufficiently thin sheets mechanical instabilities triggered under uniaxial tension can be exploited to create complex 3D patterns and even to guide the formation of permanent folds. We also find that the morphology of the instability-induced patterns is strongly affected by the loading direction [see Figs. 1(c) and 1(d) and movies 1 in the Supplemental Material [37]), pointing to an effective strategy to realize functional surfaces characterized by a variety of architectures.

We start by experimentally investigating the effect of the sheet thickness t and hinge width δ on the response of the system subjected to uniaxial tension along the square diagonals [i.e. for $\gamma = 45°$—Fig. 1(c)]. Specimens are fabricated by laser cutting an array of 3×8 mutually perpendicular cuts [see Fig. 2(b)] into plastic sheets (Artus Corporation, NJ) with Young's modulus $E = 4.33$ GPa and Poisson's ratio $\nu \simeq 0.4$ (see Supplemental Material:

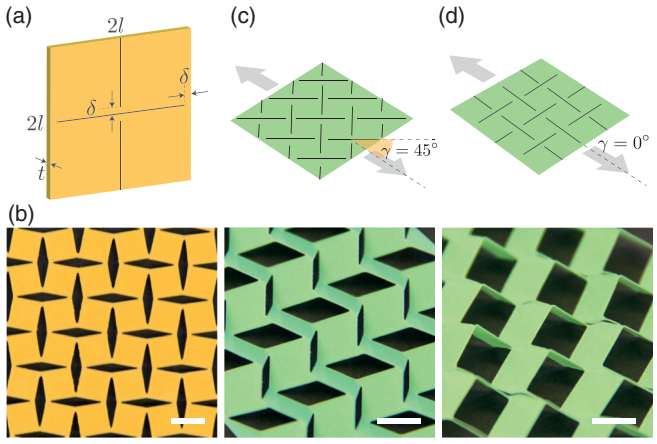

FIG. 1. (a) Schematic of the system: an elastic sheet of thickness t perforated with a square array of mutually orthogonal cuts. (b) In the thick limit (i.e., for large values of t/δ) the perforated sheet deforms in plane and identically to a network of rotating squares [28]. (c)–(d) For sufficiently small values of t/δ mechanical instabilities triggered under uniaxial tension result in the formation of complex 3D patterns, which are affected by the loading direction. The 3D patterns obtained for $\gamma = 45°$ and $\gamma = 0°$ are shown in (c) and (d), respectively. Scale bars: 6 mm.

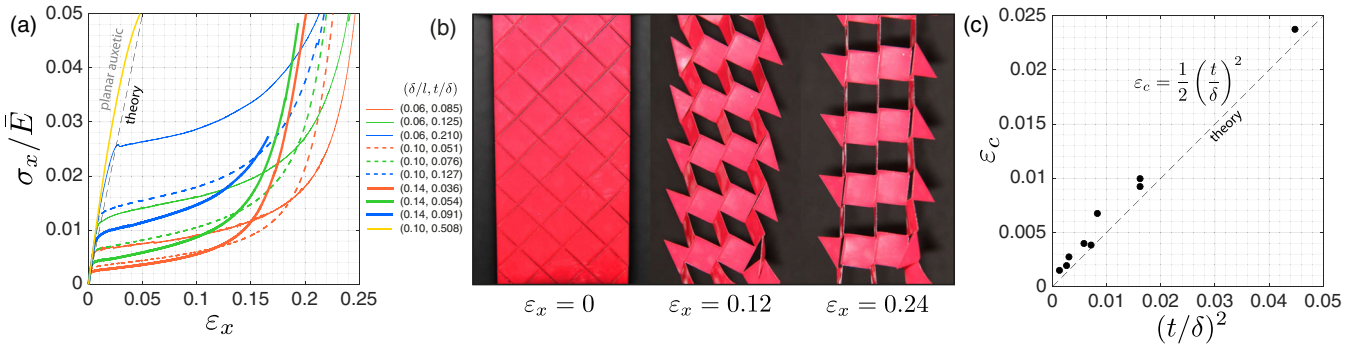

FIG. 2. (a) Experimental stress-strain curves for perforated sheets characterized by different normalized hinge width δ/l and normalized sheet thickness t/δ for $\gamma = 45°$. Note that the stress is normalized by the effective in-plane Young's modulus $\bar{E} = 2/3E(\delta/l)^2$. (b) Snapshots of the sample with $\delta/l = 0.06$ and $t/\delta \simeq 0.085$ at $\varepsilon_x = 0$, 0.12, and 0.24. (c) Critical strain ε_c as a function of $(t/\delta)^2$ as obtained from experiments (markers) and predicted analytically (dashed line).

Experiments [37]). In Fig. 2(a), we report the experimental stress-strain responses for 10 samples characterized by different values of normalized thickness t/δ and normalized hinge width δ/l.

First, it is apparent that the initial response for all samples is linear. At this stage, all hinges bend in-plane, inducing pronounced rotations of the square domains [Fig. 1(b)], which result in large negative values of the macroscopic Poisson's ratio [29,30]. As such, the stiffness of the perforated sheets, $\bar{E}$, is governed by the in-plane flexural deformation of the hinges and it can be shown that (see Supplemental Material: Analytical Exploration [37])

$$\bar{E} = \frac{\sigma_x}{\varepsilon_x} = \frac{2}{3}E\left(\frac{\delta}{l}\right)^2. \tag{1}$$

Second, for the thin samples (i.e., $t/\delta \ll 1$), the curves reported in Fig. 2(a) also show a sudden departure from linearity to a plateau stress caused by the out-of-plane buckling of the hinges. Such buckling in turn induces out-of-plane rotations of both the square domains and the cuts, which arrange to form a 3D pattern reminiscent of a misaligned Miura-ori [38] with an alternation of square solid faces (corresponding to the square domains) and rhombic open ones (defined by the cuts) [see Fig. 1(c), Fig. 2(b) at $\varepsilon_x = 0.12$ and movie 2 in the Supplemental Material [37]]. To characterize the critical strain, ε_c, at which the instability is triggered, we start by noting that since the stress immediately after instability is almost constant, the contribution of out-of-plane strain energy $\mathcal{U}_o$ should be linear in ε_x, (see Supplemental Material: Analytical Exploration [37])

$$\mathcal{U}_o(\varepsilon_x) = \bar{E}\varepsilon_c(\varepsilon_x - \varepsilon_c). \tag{2}$$

Moreover, assuming that the square domains remain rigid and that the deformation localizes at the hinges which can be modeled as flexural beam segments, $\mathcal{U}_o$ can also be written as

$$\mathcal{U}_o(\varepsilon_x) = 8\frac{1}{8l^2t}\int_0^\delta \frac{EI_o}{\rho_o^2}ds = \frac{1}{3}E\left(\frac{t}{l}\right)^2\theta_o^2, \tag{3}$$

where $I_o = \delta t^3/12$, $\rho_o = \delta/2\theta_o$, and $2\theta_o$ is the opening angle of each cut after out-of-plane buckling, which for $\gamma = 45^0$ is approximated by

$$\theta_o^2 \simeq \varepsilon_x - \varepsilon_c. \tag{4}$$

Finally, by equating Eqs. (2) and (3) we find that

$$\varepsilon_c \simeq \frac{1}{2}\left(\frac{t}{\delta}\right)^2, \tag{5}$$

which despite the simplifications made, compares very well with our experimental results [Fig. 2(c)] and numerical simulations [Fig. S6]. Note that a similar expression for the critical strain has been previously obtained for kirigami patterns comprising parallel cuts in a centered rectangular arrangement [23].

Third, for large enough values of the applied strain ε_x, the stress σ_x rises sharply again. This regime starts when the square domains align [Fig. 2(b) at $\varepsilon_x = 0.24$] and the deformation mechanism of the hinges switches from bending dominated to stretching dominated. At this stage, localized zones of intense strain (of plastic nature) develop in the hinges and result in the formation of permanent folds. Although we start with a flat elastic sheet with an embedded array of cuts (i.e., a perforated sheet), by largely stretching it we form a system that comprises a periodic distribution of both cuts and folds (i.e., a kirigami sheet). In particular, we note that our kirigami sheets possess several deformation characteristics of the Miura-ori [2,3] and zigzag-base folded kirigami [12,13] (see movie 3 in Supplemental Material [37]), as (i) they are flat foldable [Fig. 3(a)], (ii) they form a saddle shape with a negative Gaussian curvature upon nonplanar bending [Fig. 3(b)], and (iii) they can be twisted under antisymmetric out-of-plane deformation, [Fig. 3(c)]. However, in contrast to the

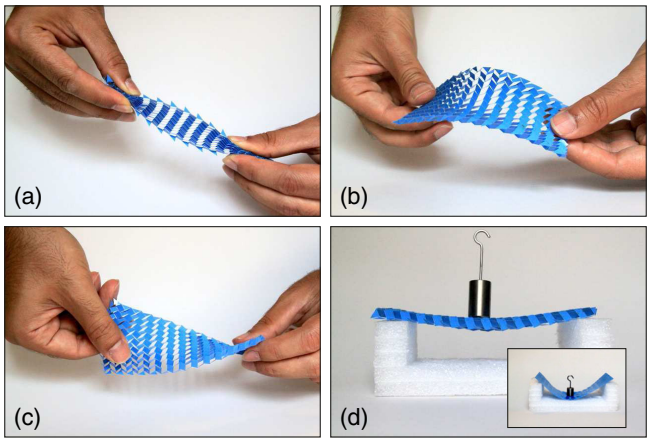

FIG. 3. The buckling-induced Miura kirigami sheet (a) is flat foldable, (b) forms a saddle shape with a negative Gaussian curvature upon nonplanar bending, (c) twists under antisymmetric out-of-plane deformation, and (d) has much higher bending rigidity than the corresponding flat perforated sheet (inset). Note that the 127 μm thick Miura kirigami sheet shown here supports a 20 g weight.

Miura-ori, misaligned Miura-ori and zigzag-base folded kirigami, the macroscopic Poisson's ratio of our kirigami sheets is positive (see movie 4 in the Supplemental Material [37]). This is the result of the fact that not all the faces are rigid. As such, the applied tensile deformation not only results in the rotation of the faces about the connecting ridges, but also in the deformation of those defined by the cuts, allowing lateral contraction of the structure. It is also noteworthy that, differently from the misaligned Miura-ori that can only be folded to a plane, the additional degree of freedom provided by the open cuts allow the Miura kirigami to be laterally flat foldable [movie 4]. Finally, we note that our Miura kirigami structures have higher bending rigidity than the corresponding flat perforated sheet [see Fig. 3(d) and Movie 3 in Supplemental Material [37]].

Having determined that instabilities in thin sheets with an embedded array of mutually perpendicular cuts can be harnessed to form complex 3D patterns, we further explore the design space using finite element (FE) analyses (See Supplemental Material: FE Simulations [37]). We start by numerically investigating the response of finite size samples stretched along the square diagonals (i.e., $\gamma = 45°$) and find excellent agreement with the experimental results (Fig. S5 and Movie 2 in the Supplemental Material [37]). This validates the numerical analyses and indicates that they can be effectively used to explore the response of the system. First, we use the simulations to understand how plastic deformation evolves. By monitoring the distribution of the von Mises stress within the sheets, we find that plastic deformation initiates at the tip of hinges well after the buckling onset [see Figs. S6 and S9] and then gradually expand to fully cover the hinges when the sample is fully stretched and the deformation mechanism changes from bending dominated to stretching dominated. Second, we numerically explore the effect of different loading conditions and find that uniaxial tension is the ideal one to

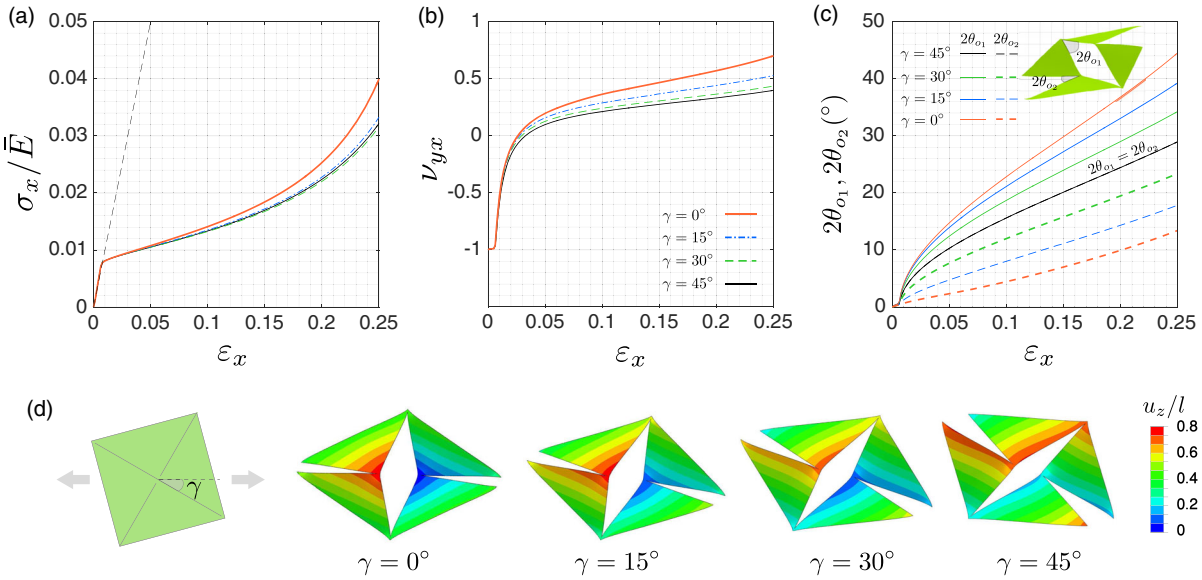

FIG. 4. Effect of loading direction γ on the mechanical response of the perforated sheets. Evolution of the (a) normalized stress $\sigma_x/\bar{E}$, (b) the in-plane macroscopic Poisson's ratio ν_{yx} and (c) the opening angle of cuts $2\theta_{o_1}$ and $2\theta_{o_2}$ as a function of the applied strain ε_x for different values of γ. Note that ν_{yx} is negative only for $\varepsilon_x < \varepsilon_c$ (as at this stage the deformation of the structure is purely planar and identical to that of a network of rotating squares) and that it increases sharply and reaches positive values once the instability is triggered. (d) Numerical snapshots of 3D patterns obtained at $\varepsilon_x = 0.125$ for different values of γ. The contours shows the normalized out-of-plane displacements.

trigger the formation of well-organized out-of-plane patterns in our perforated sheets [see Fig. S7]. Third, we investigate the effect of the loading direction by simulating the response of periodic unit cells. In Fig. 4(a) we report the stress-strain responses obtained numerically for perforated sheets characterized by $t/\delta = 0.127$ and $\delta/l = 0.04$ loaded uniaxially for $\gamma = 0°$, 15°, 30°, and 45°. Our results indicate that the mechanical response of the perforated sheets under uniaxial tension is minimally affected by the loading direction. In fact, the evolution of both stress [Fig. 4(a)] and macroscopic in-plane Poisson's ratio [Fig. 4(b)] are similar for different values of γ. By contrast, we find that the morphology of the 3D patterns induced by the instability is significantly affected by γ [Figs. 4(c) and 4(d)]. As the loading directions varies from $\gamma = 45°$ to $\gamma = 0°$, the symmetry in the opening angle of the two sets of perpendicular cuts breaks. While for $\gamma = 45°$ all cuts open equally (i.e., $\theta_{o1} = \theta_{o2}$), as we reduce γ, one set becomes wider (i.e., θ_{o1} monotonically increases) and the other progressively narrower (i.e., θ_{o2} monotonically decreases) [Fig. 4(c)]. In the limit case of $\gamma = 0°$ one set of cuts remains almost closed and a 3D cubic pattern emerges after buckling [Fig. 1(d), movie 5]. Furthermore, permanent folds with direction controlled by γ can be introduced by largely stretching the perforated sheets. As such, by controlling the loading direction a variety of kirigami sheets can be formed [movie 6]. While all of them are laterally flat foldable, we find that by increasing γ from 0° to 45° the resulting kirigami sheets have higher bending rigidity and their Gaussian curvature varies from zero (for $\gamma = 0°$) to large negative values (for $\gamma = 45°$). Furthermore, by increasing γ, the resulting kirigami sheets become more compliant under torsion (movie 6 in the Supplemental Material [37]).

In summary, our combined experimental, analytical, and numerical study indicates that buckling in thin sheets perforated with a square array of cuts and subjected to uniaxial tension can be exploited to form 3D patterns and even create periodic arrangements of permanent folds. While buckling phenomena in cracked thin plates subjected to tension have traditionally been regarded as a route toward failure [39], we show that they can also be exploited to transform flat perforated sheets to kirigami surfaces. Our buckling-induced strategy not only provides a simple route for manufacturing kirigami sheets, but can also be combined with optimization techniques to design perforated patterns capable of generating desired complex 3D surfaces under external loading [9,11,40]. Finally, since the response of our perforated sheets is essentially scale-free, the proposed *pop-up* strategy can be used to fabricate kirigami sheets over a wide range of scales, from transformable meter-scale architectures to tunable nanoscale surfaces [24,41].

K. B. acknowledges support from the National Science Foundation under Grant No. DMR-1420570 and CMMI-1149456. A. R. also acknowledges the financial support provided by Swiss National Science Foundation (SNSF) under Grant No. 164648. The authors thank Bolei Deng for fruitful discussions, Yuerou Zhang for assistance in laser cutting, and Matheus Fernandes for proofreading the manuscript.

*Corresponding author.
bertoldi@seas.harvard.edu

[1] L. Mahadevan and S. Rica, Science **307**, 1740 (2005).
[2] M. Schenk and S. D. Guest, Proc. Natl. Acad. Sci. U.S.A. **110**, 3276 (2013).
[3] Z. Y. Wei, Z. V. Guo, L. Dudte, H. Y. Liang, and L. Mahadevan, Phys. Rev. Lett. **110**, 215501 (2013).
[4] T. Tachi, J. Mec. Des. **135**, 111006 (2013).
[5] J. L. Silverberg, A. A. Evans, L. McLeod, R. C. Hayward, T. Hull, C. D. Santangelo, and I. Cohen, Science **345**, 647 (2014).
[6] H. Yasuda and J. Yang, Phys. Rev. Lett. **114**, 185502 (2015).
[7] J. L. Silverberg, J-H. Na, A. A. Evans, B. Liu, T. C. Hull, C. D. Santangelo, R. J. Lang, R. C. Hayward, and I. Cohen, Nat. Mater. **14**, 389 (2015).
[8] J. T. B. Overvelde, T. A. de Jong, Y. Shevchenko, S. A. Becerra, G. M. Whitesides, J. C. Weaver, C. Hoberman, and K. Bertoldi, Nat. Commun. **7**, 10929 (2016).
[9] L. H. Dudte, E. Vouga, T. Tachi, and L. Mahadevan, Nat. Mater. **15**, 583 (2016).
[10] T. Castle, Y. Cho, X. Gong, E. Jung, D. M. Sussman, S. Yang, and R. D. Kamien, Phys. Rev. Lett. **113**, 245502 (2014).
[11] D. M. Sussman, Y. Cho, T. Castle, X. Gong, E. Jung, S. Yang, and R. D. Kamien, Proc. Natl. Acad. Sci. U.S.A. **112**, 7449 (2015).
[12] M. Eidini and G. H. Paulino, Sci. Adv. **1**, e1500224 (2015).
[13] M. Eidini, Ext. Mech. Lett. **6**, 96 (2016).
[14] T. Castle, D. M. Sussman, M. Tanis, and R. D. Kamien, Sci. Adv. **2**, e1601258 (2016).
[15] B. G. Chen, B. Liu, A. A. Evans, J. Paulose, I. Cohen, V. Vitelli, and C. D. Santangelo, Phys. Rev. Lett. **116**, 135501 (2016).
[16] Y. Tang and J. Yin, Ext. Mech. Lett., DOI: 10.1016/j.eml.2016.07.005.
[17] K. A. Seffen, Phys. Rev. E **94**, 033003 (2016).
[18] Z. Song, X. Wang, C. Lv, Y. An, M. Liang, T. Ma, D. He, Y-J. Zheng, S-Q. Huang, H. Yu, and H. Jiang, Sci. Rep. **5**, 10988 (2015).
[19] T. C. Shyu, P. F. Damasceno, P. M. Dodd, A. Lamoureux, L. Xu, M. Shlian, M. Shtein, S. C. Glotzer, and N. A. Kotov, Nat. Mater. **14**, 785 (2015).
[20] M. K. Blees, A. W. Barnard, P. A. Rose, S. P. Roberts, K. L. McGill, P. Y. Huang, A. R. Ruyack, J. W. Kevek, B. Kobrin, D. A. Muller, and P. L. McEuen, Nature (London) **524**, 204 (2015).
[21] A. Lamoureux, K. Lee, M. Shlian, S. R. Forrest, and M. Shtein, Nat. Commun. **6**, 8092 (2015).
[22] D. Norman, V&A Conserv. J. **9**, 10 (1999).
[23] M. Isobe and K. Okumura, Sci. Rep. **6**, 24758 (2016).
[24] C. Wu, X. Wang, L. Lin, H. Guo, and Z. L. Wang, ACS Nano **10**, 4652 (2016).

[25] Y. Zhang, Z. Yan, K. Nan, D. Xiao, Y. Liu, H. Luan, H. Fu, X. Wang, Q. Yang, J. Wang, W. Ren, H. Si, F. Liu, L. Yang, H. Li, J. Wang, X. Guo, H. Luo, L. Wang, Y. Huang, and J. A. Rogers, Proc. Natl. Acad. Sci. U.S.A. **112**, 11757 (2015).
[26] Z. Yan, F. Zhang, J. Wang, F. Liu, X. Guo, K. Nan, Q. Lin, M. Gao, D. Xiao, Y. Shi, Y. Qiu, H. Luan, J. H. Kim, Y. Wang, H. Luo, M. Han, Y. Huang, Y. Zhang, and J. A. Rogers, Adv. Funct. Mater. **26**, 2629 (2016).
[27] R. M. Neville, F. Scarpa, and Alberto Pirrera, Sci. Rep. **6**, 31067 (2016).
[28] J. N. Grima and K. E. Evans, J. Mater. Sci. Lett. **19**, 1563 (2000).
[29] A. A. Vasiliev, S. V. Dmitriev, Y. Ishibashi, and T. Shigenari, Phys. Rev. B **65**, 094101 (2002).
[30] J. N. Grima, A. Alderson, and K. E. Evans, Phys. Status Solidi B **242**, 561 (2005).
[31] S. Shan, S. H. Kang, Z. Zhao, L. Fang, and K. Bertoldi, Ext. Mech. Lett. **4**, 96 (2015).
[32] Y. Cho, J.-H. Shin, A. Costa, T. A. Kim, V. Kunin, J. Li, S. Yeon Lee, S. Yang, H. N. Han, I.-S. Choi, and D. J. Srolovitz, Proc. Natl. Acad. Sci. U.S.A. **111**, 17390 (2014).
[33] R. Gatt, L. Mizzi, J. I. Azzopardi, K. M. Azzopardi, D. Attard, A. Casha, J. Briffa, and J. N. Grima, Sci. Rep. **5**, 8395 (2015).
[34] Y. Suzuki, G. Cardone, D. Restrepo, P. D. Zavattieri, T. S. Baker, and A. F. Tezcan, Nature (London) **533**, 369 (2016).
[35] J. N. Grima, E. Manicaro, and D. Attard, Proc. R. Soc. A **467**, 439 (2011).
[36] A. Rafsanjani and D. Pasini, Ext. Mech. Lett. **9**, 291 (2016).
[37] See Supplemental Material at http://link.aps.org/supplemental/10.1103/PhysRevLett.118.084301 which includes Refs. [28–30], supporting movies, an analytical exploration, details of the FE simulations, and a description of the experiments.
[38] K. Saito, A. Tsukahara, and Y. Okabe, Proc. R. Soc. A **472**, 20150235 (2016).
[39] G. F. Zielsdorff and R. L. Carlson, Eng. Fract. Mech. **4**, 939 (1972).
[40] M. Konaković, K. Crane, B. Deng, S. Bouaziz, D. Piker, and M. Pauly, ACM Trans. Graph. **35**, 89 (2016).
[41] F. Cavallo, Y. Huang, E. W. Dent, J. C. Williams, and M. G. Lagally, ACS Nano **8**, 12219 (2014).